sustainability

MDPI

Article

Wind Energy Assessment in Forested Regions Based on the Combination of WRF and LSTM-Attention Models

Guanghui Che [1], Daocheng Zhou [1], Rui Wang [2], Lei Zhou [3], Hongfu Zhang [1,*] and Sheng Yu [4,*]

[1] School of Civil Engineering and Transportation, Northeast Forestry University, Harbin 150040, China; cghccc123@163.com (G.C.); hitzdc@126.com (D.Z.)
[2] Jinan Park Development Service Center, Jinan 250000, China; ruiw123@126.com
[3] Department of Mechanical Engineering, The Hong Kong Polytechnic University, Kowloon, Hong Kong 999077, China; lzhouau@connect.ust.hk
[4] School of Civil and Environmental Engineering, Harbin Institute of Technology, Shenzhen 518055, China
* Correspondence: zhanghongfu@nefu.edu.cn (H.Z.); yusheng2021@hit.edu.cn (S.Y.)

Abstract: In recent years, the energy crisis has become increasingly severe, and global attention has shifted towards the development and utilization of wind energy. The establishment of wind farms is gradually expanding to encompass forested regions. This paper aims to create a Weather Research and Forecasting (WRF) model suitable for simulating wind fields in forested terrains, combined with a long short-term time (LSTM) neural network enhanced with attention mechanisms. The simulation focuses on capturing wind characteristics at various heights, short-term wind speed prediction, and wind energy assessment in forested areas. The low-altitude observational data are obtained from the flux tower within the study area, while high-altitude data are collected using mobile radar. The research findings indicate that the WRF simulations using the YSU boundary layer scheme and MM5 surface layer scheme are applicable to forested terrains. The LSTM model with attention mechanisms exhibits low prediction errors for short-term wind speeds at different heights. Furthermore, based on the WRF simulation results, a wind energy assessment is conducted for the study area, demonstrating abundant wind energy resources at the 150 m height in forested regions. This provides valuable support for the site selection in wind farm development.

Keywords: forested region; WRF model; long short-term time neural network; wind field simulation; wind energy assessment

Citation: Che, G.; Zhou, D.; Wang, R.; Zhou, L.; Zhang, H.; Yu, S. Wind Energy Assessment in Forested Regions Based on the Combination of WRF and LSTM-Attention Models. *Sustainability* **2024**, *16*, 898. https://doi.org/10.3390/su16020898

Academic Editor: Giovanni Gualtieri

Received: 4 December 2023
Revised: 12 January 2024
Accepted: 17 January 2024
Published: 20 January 2024

1. Introduction

Global energy scarcity and air pollution problems are becoming increasingly serious, and the development of clean, renewable energy has become a top priority. Wind power is an important form of renewable energy utilization, which has seen a steady and rapid growth in installed capacity worldwide in recent years [1]. For wind farm development, it is important to assess the wind power generation potential at a given location or area to determine the capacity of the wind resource to generate power within the available time frame of wind duration [2,3]. Therefore, efficient and accurate regional wind field simulation and wind resource assessment are significant for developing and setting up wind farms. As the large-scale development of wind power continues, most current wind farms are still concentrated in simple and flat areas. Although complex terrain is rich in wind energy resources, high turbulence, and wind shear due to its topographic complexity, it makes wind field simulation and wind conditions more difficult to predict accurately [4,5]. In forested regions with relatively complex terrain, extensive vegetation coverage results in a rough terrain surface. Simultaneously, the irregular terrain causes the wind field to become complex and unstable, thereby affecting the distribution of wind energy resources [6]. These factors pose challenges to conducting accurate wind energy resource assessments in forested terrain.

The development of wind farms necessitates an initial assessment of wind energy resources, and on-site wind measurements at locations of interest are typically the most reliable approach for regional wind field studies [7,8]. Generally, a minimum of one year of on-site measurements is recommended prior to wind farm development [9]. However, due to various constraints—such as high costs, construction height limitations, and data transmission issues—especially in forested areas with relatively complex terrain, relying only on measured data such as meteorological stations for wind resource assessment is not sufficient to meet the current needs of wind energy development. With the rapid development of computer technology, more and more scholars are combining numerical simulation technology with wind field simulation research on complex terrain and applying it to wind resource assessment research. The Water Analysis Simulation Program (WAsP) linear model can be used to estimate the vertical and horizontal distribution of wind speeds in a region [10], but it does not accurately reflect ground friction and thermal effects for regions of complex terrain. Large eddy simulation (LES) in Computational fluid Dynamics(CFD) can accurately capture the details of the flow field [11,12] and is also widely used in the simulation of wind farms in complex terrain [13,14]. However, since CFD models, whether in simulating wind fields or assessing wind energy, rely solely on predetermined parameter values and do not account for time-varying meteorological conditions, the impact of meteorological factors on wind farms cannot be adequately represented within the framework of CFD models.

The WRF model is the most widely used NWP model, which is capable of realizing high-resolution large-area wind field simulation, as well as its high adaptability to complex terrain and computational efficiency, and has made some progress in wind field simulation and wind energy assessment in forested regions. Prosper Miguel et al. [15] used the WRF model to conduct a wind energy resource assessment for the Coruxeiras coastal wind farm and tested the effectiveness of WRF in calculating the energy yield of complex terrain wind farms. Soklin Tuy et al. [16] assessed and mapped Cambodia's offshore wind resources and power potential using the WRF model and Sentinel-1 L2 OCN imagery. Xu et al. [17] carried out WRF simulations and developed a WRF-based multistep wind speed prediction model for wind farms located in Sichuan, China. Liu et al. [6] carried out simulations of wind fields in forested areas using localized leaf area index and roughness length replacement WRF surface data. Quimbayo-Duarte et al. [18] assessed the impact of forest parameterization on boundary layer flow simulations over moderately complex terrain using WRF-LES. In recent years, artificial intelligence technology has made significant progress, and LSTM neural networks have especially been successfully applied in various fields [19,20]. Using the LSTM neural network for wind power prediction not only saves time, but also improves the accuracy of prediction [21].

Currently, researchers have conducted studies on wind characteristics in forested regions, such as wind profiles, but there has been limited research focused on short-term wind speed prediction and wind energy resource assessment specifically tailored for forested regions. This paper aims to optimize the parameterization scheme for WRF simulations in forested regions, utilize the LSTM neural network for future wind speed prediction, and conduct a wind energy resource assessment in forested regions. The subsequent sections of this paper are outlined as follows: Section 2 describes the study region, the source of field measurements, the development of the WRF model, and the methodology of the LSTM neural network. Section 3 describes the selection of the optimal parameterization scheme of the WRF and the results of the temporal prediction performed by the LSTM, as well as the assessment of the wind energy resources in the forested regions. Section 4 summarizes the main conclusions. The results of this research can support the development of wind energy assessment and short-term wind speed prediction in forested terrain.

2. Methodology and Data

As mentioned above, selecting parameterization schemes in the WRF model is crucial for simulating the wind field in forested regions with complex terrain. Therefore, to conduct

more accurate wind field simulations, the first step involves simulating the wind field in forested regions by selecting different combinations of WRF parameterization schemes. The optimal parameterization scheme is determined through error analysis of the simulation results, and long-term wind field simulations are carried out. Finally, the simulated results are input into an LSTM neural network, enabling further training of the neural network for short-term wind speed predictions in the wind field.

2.1. Study Region and Field Data

The study region of this research is the Mao'er Mountain region in northeastern China, which is part of the Changbai Mountain range and is located in the East Asian monsoon region, surrounded by abundant forest resources and rich wind energy potential. The low-altitude wind field observational data are obtained from the flux tower, while the observational data for the wind field at altitudes of 50 m and above are acquired from lidar measurements. The wind measurement system of the flux tower consists of five WindMaster three-dimensional ultrasonic anemometers from the British company GILL, a data logger (Campbell CR6) from the United States, and a power supply system. The wind measurement site is located within the Mao'er Mountain Laoyeling National Ecological Observatory Station of Northeast Forestry University in Mao'ershan Town, Shangzhi City, Harbin, Heilongjiang Province, as shown in Figure 1a. The mobile wind measurement lidar selected is the vertical-type lidar model WindMast WP350 developed by RayMetrics. This lidar operates based on the principle of optical pulse coherent Doppler frequency shift detection. It has a maximum vertical observation range of 20 to 350 m, a wind speed measurement range of 0 to 75 m/s, wind speed accuracy of $\leq$0.1 m/s, and a sampling frequency of 10 Hz. The lidar was mounted at a hillside (45.403825° N, 127.659458° E) at an altitude of 389 m. It measured wind speed at heights ranging from 50 m to 200 m above the ground, with a sampling frequency of 10 Hz, as shown in Figure 1b.

(**a**) (**b**)

Figure 1. Observational equipment for measured data: (**a**) The flux tower. (**b**) Mobile wind measurement lidar.

2.2. WRF Model Configuration

This study focuses on the Mao'er Mountain region as the research region and establishes a wind field forecasting model using the WRF model. WRF version 4.3.1 is employed for wind field simulations. The WRF model allows for the selection of either one-way or two-way grid nesting, where "one-way" and "two-way" refer to how the coarse domain and the fine domain interact. In the case of two-way nesting, the model enables the exchange of information between the parent domain and the nested domain, facilitating a more effective capture of atmospheric processes across different spatial scales [22,23]. All simulations in this study are set up as a 4-layer two-way nesting scheme, with the

innermost nested domain covering the study region. The simulation center is located at a latitude of 45.40° N and a longitude of 127.66° E. The horizontal resolutions are set at 9 km (101 × 101), 3 km (109 × 109), 1 km (109 × 109), and 333 m (109 × 109), respectively, and the study region is shown in Figure 2. The vertical configuration consists of 58 layers, with the bottom heights of the first seven layers above the ground set at 12.2 m, 36.6 m, 60.6 m, 84.1 m, 107.8 m, 142.9 m, and 189.6 m, respectively. The model top is set at a constant pressure level of 5000 Pa. The modeling employed Lambert projection, and the model initialization as well as boundary layer data were sourced from the National Centers for Environmental Prediction (NCEP) reanalysis data (FNL). [24]. In order to minimize model systematic errors, the simulation results were discarded for the first and second 12 h of data before post-processing analysis.

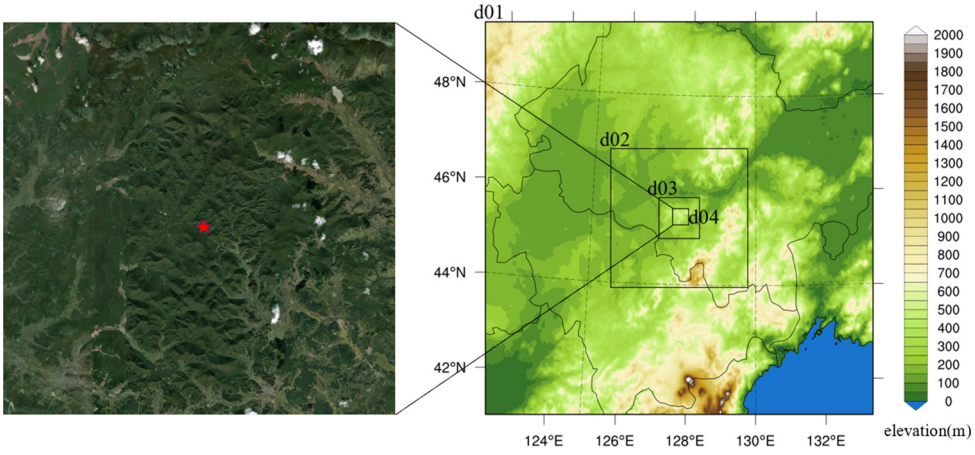

Figure 2. Topographic maps of model nested domains and innermost nested domains. (Asterisks indicate measured locations).

The selection of parameterization schemes is crucial for WRF simulations of near-surface wind fields in forested regions [25]. The following four schemes were set up based on the selected study region, and a 5-day WRF simulation was conducted from 00:00 on 22 November 2020, to 23:00 on 26 November 2020. The objective was to analyze the specific impacts of different cumulus cloud schemes, longwave and shortwave radiation, planetary boundary layer schemes, surface layer schemes, and land surface parameterization schemes on WRF simulations, as shown in Table 1. Setup1 and Setup2 were configured to analyze the impact of the improved cumulus parameterization scheme, the Kain–Fritsch cumulus scheme (abbreviated as KFC) [26], and the longwave and shortwave radiation scheme RRTMG [27], in comparison with the Kain-Fritsch cumulus parameterization scheme (KF) [28], and longwave and shortwave radiation scheme RRTM [29] on the simulation of wind fields. Setup3 and Setup4 are configured to analyze the impact of planetary boundary layer and surface layer schemes on wind field simulation. Since the planetary boundary layer and surface layer schemes are chosen as pairs, the YSU planetary boundary layer [30] and MM5 surface layer [31], as well as the MYJ planetary boundary layer [32] and Eta surface layer [33], are selected as control groups based on their performance in previous wind field simulations. Setup2 and Setup4 serve as control groups to analyze the impact of land surface parameterization schemes Noah [34] and NoahMP [35] on wind field simulation. The microphysics parameterization scheme used is WSM6 [36].

After the analysis of the influence of the parameterization scheme on the simulation effect (for details, please see Section 3.1), Setup3 is selected as the optimal parameterization scheme for the selected study area, and the WRF simulation is conducted for the study area for 30 days from 0:00 on 1 December 2020, to 0:00 on 31 December 2020, for the study region. The simulation results were compared with the measured values (below 50 m with the measured values from the flux tower and above 50 m with the measured values from the radar).

Table 1. Model configuration options used for WRF simulations.

	Setup1	Setup2	Setup3	Setup4
Microphysics	WSM6	WSM6	WSM6	WSM6
Cumulus Parameterization	KF	KFC	KFC	KFC
Longwave Radiation	RRTM	RRTMG	RRTMG	RRTMG
Longwave Radiation	Dudhia	RRTMG	RRTMG	RRTMG
Planetary Boundary layer	MYJ	MYJ	YSU	MYJ
Surface Layer	Eta	Eta	MM5	Eta
Land Surface	Noah	Noah	NoahMP	NoahMP

2.3. Machine Learning Model Configurations

The output data from the innermost domain (d04) of the WRF model is used to drive the deep learning model, and the long short-term memory neural network (LSTM) is selected for short-term wind speed prediction in this study. LSTM is a recurrent neural network (RNN) proposed by Hochreiter and Schmidhuber [37], which adds forgetting and reinforcement learning based on RNN. It is a time-recursive neural network suitable for processing and predicting events with very long intervals and delays in the time series. It is widely used in language recognition and text prediction [38]. The main difference between LSTM and traditional RNN is the inclusion of input gate i_t, forgetting gate f_t, output gate o_t, and internal memory units $\widetilde{C}_t$. The input gate controls the input x_t and the extent to which the currently computed state is updated to the memory cell; the forgetting gate controls the input x_t and the extent to which the output h_{t-1} of the previously hidden layer is forgotten; and the output gate determines how much the input x_t and the current output h_t depend on the current memory unit. Therefore, LSTM can learn the long-term dependency and extract the complex feature relations of long-time sequences, and the cell unit structure is shown in Figure 3. Therefore, compared to the traditional neural network structure, LSTM is more capable of learning long-term dependencies and effectively extracting complex feature relationships in long time series. In addition, by adapting to the irregularity of the data, it is made more effective in learning the trends and periodic changes of the input wind field data and improves the modeling ability to accurately capture and predict the changes of the wind speed in the forest area. The LSTM cell unit structure diagram is shown in Figure 3. The attention mechanism is a mechanism inspired by how the human brain allocates attention to different aspects, which emphasizes the key parts of the data and ignores irrelevant disturbances. In LSTM neural networks, the added attentional mechanism can improve model prediction accuracy by selectively training on important inputs through weight calculation. In complex terrain areas, terrain, vegetation, and other factors often interfere with wind speed. By introducing the attention mechanism, the established neural network model can better focus on the input data related to the change in wind speed to realize the prediction of short-term wind speed at multiple heights.

Based on the above background, this paper constructs a 7-layer LSTM-Attention prediction model, which consists of an input layer, a fully connected layer, an attention layer, an LSTM layer, a bath normalization (BN) layer, a fully connected layer, and an output layer. The framework is shown in Figure 4. The specific model parameters are as follows: the dimension of the input layer is set to 3, the number of hidden units in the fully connected layer is 50, the number of neurons in the LSTM layer is 50, while tanh is used as the activation function, and the final dimension of the output layer is 1. The constructed model is able to take full advantage of the characteristics of layers such as LSTM and attention to improve the modeling and prediction of time series data, and the introduction of the BN layer and the fully connected layer also helps to optimize the training and overall performance of the model. The whole workflow is as follows: firstly, the wind speed, wind direction, and temperature data obtained from the simulation of the innermost nested domain of the WRF are subjected to standardization and normalization processes before being input into the prediction model. Subsequently, feature mapping is performed through the fully connected layer, and the attention mechanism is introduced to

calculate the attention weight assigned to each input, which is weighted and input to the LSTM layer, while the BN layer is introduced to prevent the problem of gradient explosion or disappearance. Finally, the LSTM output is integrated through the fully connected layer to output the predicted results. Such a hierarchical structure can be better adapted to wind speed prediction under forested terrain.

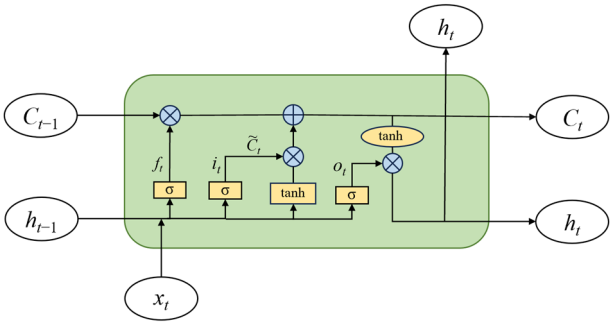

Figure 3. LSTM cell unit structure diagram.

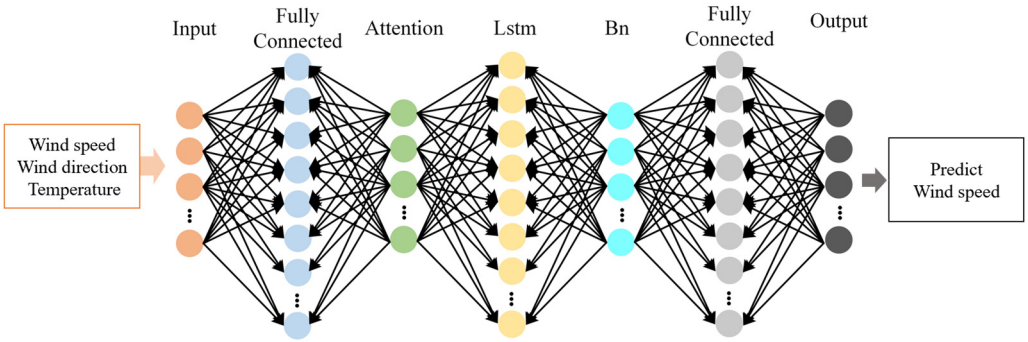

Figure 4. LSTM-Attention neural network model structure.

The detail formula can be given in the following equations:

$$f_t = \sigma\left(W_f \cdot [h_{t-1}x_t] + b_f\right) \quad (1)$$

$$i_t = \sigma(W_i \cdot [h_{t-1}x_t] + b_i) \quad (2)$$

$$\widetilde{C}_t = \tanh(W_c \cdot [h_{t-1}x_t] + b_c) \quad (3)$$

$$C_t = f_t \times C_{t-1} + i_t \times \widetilde{C}_t \quad (4)$$

$$o_t = \sigma(W_o \cdot [h_{t-1}x_t] + b_o) \quad (5)$$

$$h_t = o_t \times \tanh(C_t) \quad (6)$$

where t is the time step; x_t is the input at the current moment; σ is the sigmoid function; f_t, i_t, and o_t have values ranging from 0 to 1 and are the outputs of the three σs; W_f, W_i, W_c, and W_o are the weights used to connect the previous cell with the new input x_t and the output h_{t-1}; and b_f, b_i, b_c, and b_o are the corresponding bias.

In the process of WRF simulation, there is a certain dependence and correlation between the later and earlier values of the simulation results, and the wind speed prediction not only relies on the latest data of meteorological elements but also obtains the general trend of the wind speed change through the earlier simulation data. In this study, the WRF simulated wind field data at three heights of 50 m, 100 m, and 150 m are inputted into the constructed LSTM-Attention model, the correlation between the data is further explored through the attention mechanism, the effects of different categories of data on the predicted wind speed are analyzed, and the data are reconstructed to predict the future wind speed

data, which is analyzed in comparison with the actual radar measured wind speed and the wind profile, enabling temporal wind speed forecasting.

2.4. Methodology for Wind Resource Assessment

The Weibull probability density distribution model is often used for regional wind resource assessment and has been found in practice to be suitable for fitting probability distributions of wind speeds at various locations for effective wind resource assessment [39,40]. Therefore, in this study, the Weibull distribution probability model is chosen to fit the probability distribution of wind speed at different heights, and its probability density function is expressed as [41]:

$$f(v) = \frac{k}{c}\left(\frac{v}{c}\right)^{k-1} \exp\left[-\left(\frac{v}{c}\right)^{k}\right] \tag{7}$$

where k is a shape parameter, determines the shape of the distribution (with larger values indicating smaller wind speed fluctuations), and generally fluctuates between 1 and 3 (a larger the value of k indicates that the wind speed fluctuation is smaller); c is a scale parameter, reflecting the average wind speed of the wind farm.

Wind power density is an important indicator for evaluating whether the wind energy resources in a region are worth developing and is calculated by the following formula:

$$\overline{w} = \frac{1}{2}\rho v^3 \tag{8}$$

where ρ is the air density (kg/m^3), and is normally a constant value of 1.225 kg/m^3; v is the wind speed (m/s); and $\overline{w}$ is the wind power density (W/m^2).

3. Results and Discussion

RMSE, *ME*, and *R* were used to validate the simulations. *RMSE* represents the sample standard deviation of the difference between the simulated and observed values, indicating the degree of dispersion of the sample; *ME* represents the average of the errors between the simulated and observed values. The smaller values of *RMSE* and *ME* prove that the simulated values are closer to the observed values. *R* represents the linear correlation between the simulated and observed values (with the value range being between 0 and 1); moreover, the closer the value of *R* is to 1, the more closely correlated the observed values are. The closer the value of *R* is to 1, the stronger the correlation between the simulated and observed values. The specific formulas for the above error evaluation indexes are as follows:

$$RMSE = \sqrt{\frac{1}{n}\sum_{i=1}^{n}(f_i - f_{obi})^2} \tag{9}$$

$$ME = \frac{1}{n}\sum_{i=1}^{n}(f_i - f_{obi}) \tag{10}$$

$$R = \frac{\sum_{i=1}^{n}\left(f_{obi} - \overline{f}_{obi}\right)\left(f_i - \overline{f_i}\right)}{\left[\sum_{i=1}^{n}\left(f_{obi} - \overline{f}_{obi}\right)^2 \sum_{i=1}^{n}\left(f_i - \overline{f_i}\right)^2\right]^{1/2}} \tag{11}$$

where i is the time point; n is the total number of time points in the simulation period; f_i is the value of simulation at a certain time point, respectively; and f_{obi} is the value of observation at a certain time point, respectively.

3.1. Results of WRF Simulations

To better simulate wind fields in forested regions, a 5-day WRF simulation was conducted for the study area from 00:00 on 22 November 2020, to 23:00 on 26 November 2020. Comparative validation of error parameters between simulated wind speeds at

various heights using different parameterization schemes and observed results are shown in Figure 5.

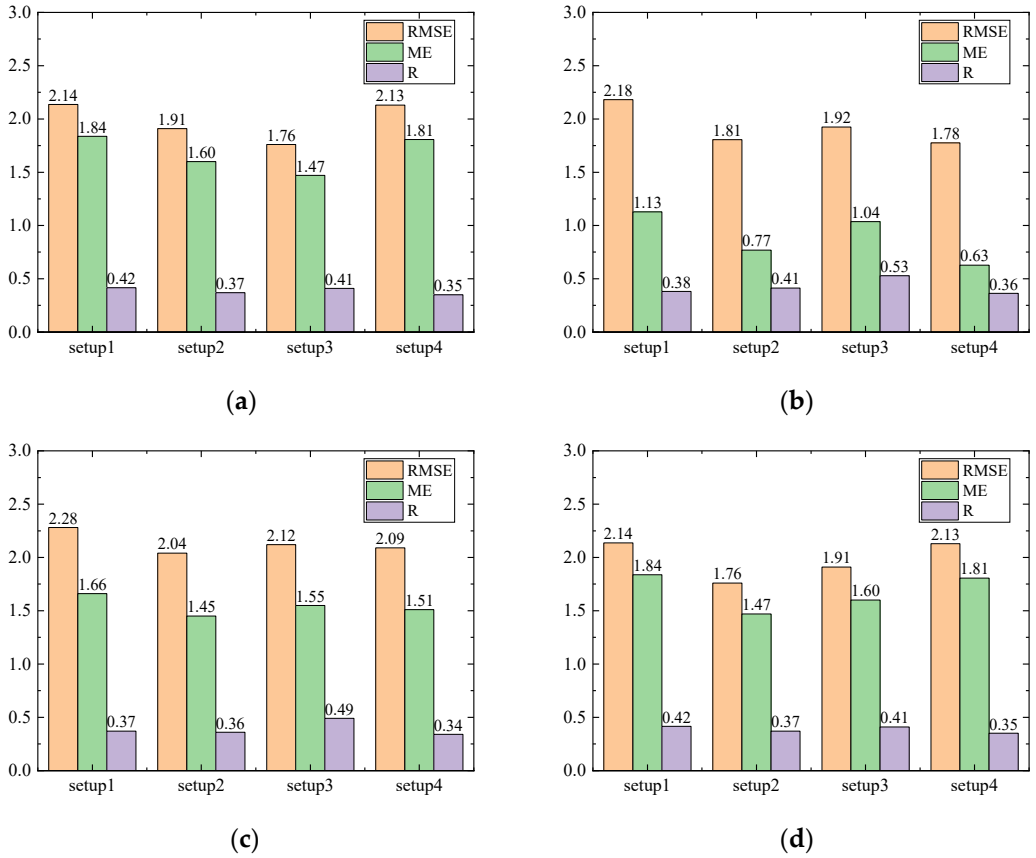

Figure 5. Comparison of simulated and observed error parameters at different heights for multiple Setups: (**a**) 10 m, (**b**) 50 m, (**c**) 100 m, and (**d**) 150 m.

The difference between Setup1 and Setup2 is that the improved KFC cumulus parameterization scheme and the RRTMG long and short wave radiation scheme are chosen for Setup2. As shown in Figure 5, it can be observed that Setup1 performs better than Setup2 at various heights. The error values *RMSE* and *ME* are reduced, and the correlation coefficient *R* is improved at a height of 50 m in Setup 1 compared to Setup2. The difference between Setup2 and Setup4 lies in the selection of the land surface scheme, which can be seen in Figure 5, indicating that the error value of Setup2 is smaller than that of Setup4 at 10 m and 100 m heights, but the error values of the two schemes at a 50 m height are closer, and the correlation coefficient of Setup4 at a 200 m height is improved compared with that of Setup1. The difference between Setup3 and Setup4 lies in selecting the planetary boundary layer and surface layer schemes. As shown in Figure 5, it can be observed that Setup3, which uses the YSU boundary layer scheme and the MM5 surface layer scheme, outperforms other parameterization schemes at multiple heights with consistently higher correlation coefficients. Therefore, Setup3 is identified as the optimal parameterization scheme suitable for the selected region, and a one-month WRF simulation is carried out based on this setup.

The simulated wind speed against the observed wind speed at each height for Setup3 is shown in Figure 6, and the comparative validation of the error parameters of the simulated and observed wind speed against the simulated results at different heights is shown in Figure 7.

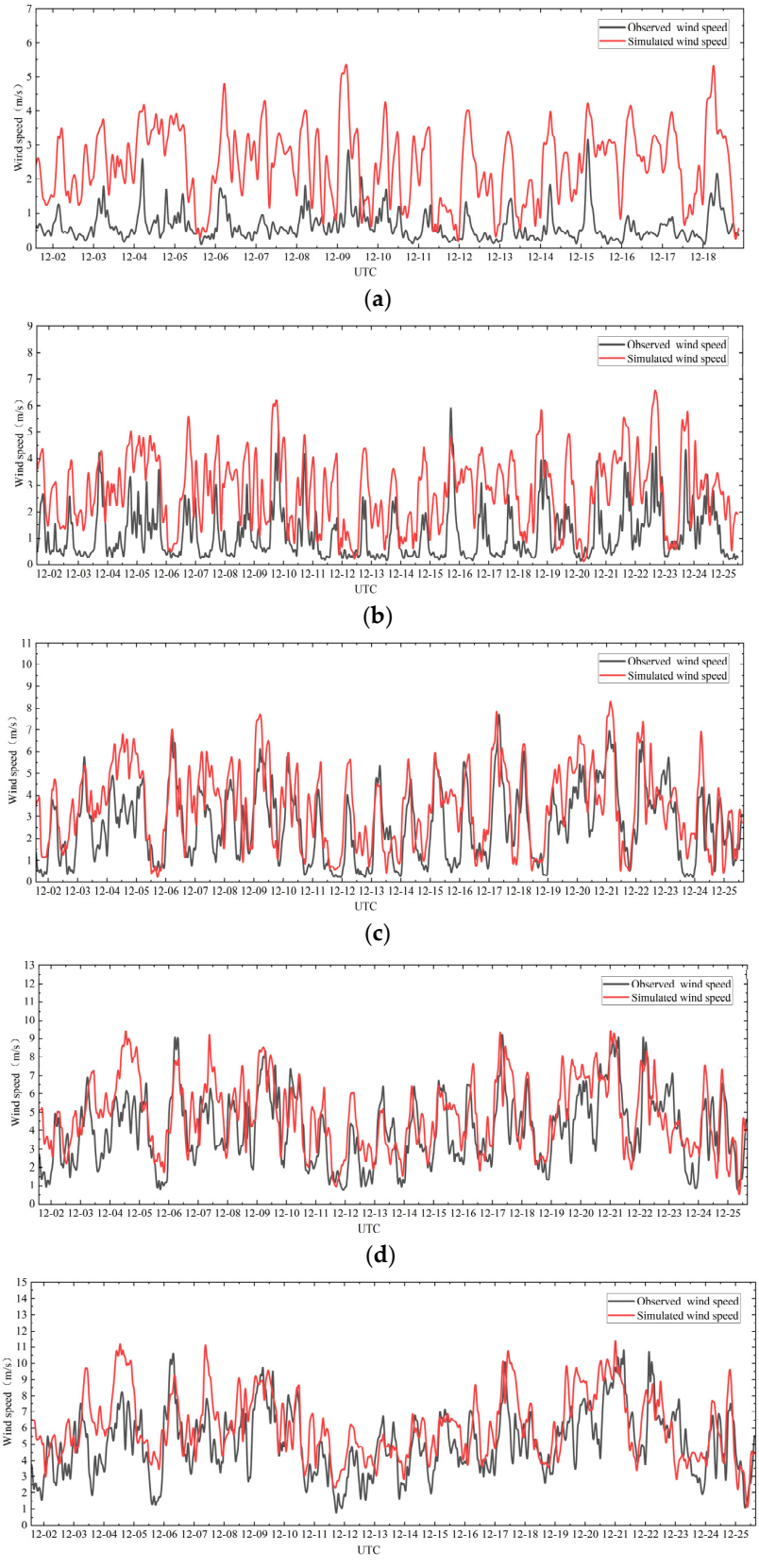

Figure 6. Comparison of simulated and observed wind speed at different heights: (**a**) 10 m, (**b**) 20 m, (**c**) 50 m, (**d**) 100 m, and (**e**) 150 m.

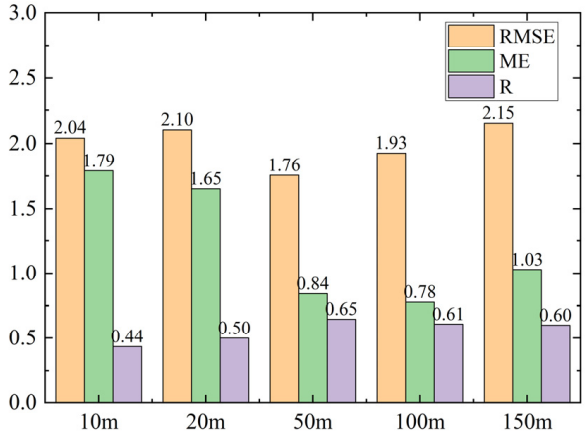

Figure 7. Comparison of simulated and observed error parameters at different heights.

Since the selected study area is located in a forested area with complex terrain, the actual wind measurement by the flux tower is blocked by the surrounding trees as seen in Figure 1a, resulting in a lower measured wind speed compared to the real wind speed. At the same time, the surface roughness of the forest area is large, and the complex terrain makes the wind speed distribution in the area more complicated. This makes the WRF model not accurate enough to capture the local terrain changes, which leads to the overestimation of wind speed. As a result, there are large numerical errors between the simulated and observed wind speeds at heights of 10 m and 20 m near the ground. As the height increases to 50 m, the shading of the flux tower by trees improves and the error between the simulated and observed wind speeds decreases significantly. The *ME* is greater than 1.5 m/s at both 10 m and 20 m heights, while the *ME* decreases to 0.84 m/s at 50 m height with a correlation coefficient *R* of 0.65, which reflects a strong linear relationship between the simulated and observed wind speeds.

Between the heights of 50 m and 150 m, the simulated wind speed curve demonstrates excellent performance in capturing the diurnal cycle and wind speed trends. From 0:00 to 12:00, the wind speed gradually increases, reaching its daily maximum, followed by the occurrence of the minimum wind speed from 12:00 to the next day's 0:00. As can be seen in Figure 6d, the observed wind speed profile on 24 December shows a slowly increasing trend at the 100 m height, eventually reaching 5.5 m/s. However, during this period, the simulated wind speed profile shows a decreasing trend and finally reaches the simulated minimum wind speed of 3 m/s for the day. Subsequently, the observed wind speed profile gradually decreases to 1 m/s after this point. This discrepancy mainly stems from the fact that the WRF model fails to adequately characterize the effects of complex terrain and forest disturbances, and thus fails to accurately capture the topographic microclimates due to the characteristics of complex terrain and forested areas. As can be seen in Figure 6e, the WRF simulation is slightly less effective at 150 m altitude compared to 50 m and 100 m altitude. The observed wind speeds vary over a much wider range, between 1 and 11 m/s, while the WRF simulation is better for wind speeds in the range of 3 to 10 m/s, with errors in the simulation for higher and lower wind speeds. This discrepancy is due to the effect of atmospheric stability on the wind simulation at higher altitudes, as well as the fact that the turbulence parameterization scheme used in the model performs differently at different altitudes, with the selected combination of parameterization schemes performing poorly in the wind simulation at an altitude of 150 m.

As shown in Figure 7, it is evident that using Setup 3, which incorporates the YSU planetary boundary layer and MM5 surface layer schemes, yields favorable simulation results for heights above 50 m. The *R* consistently exceeds 0.6, while the *ME* remains below 1 m/s. Notably, at 50 m, the *R* reaches its maximum at 0.65, accompanied by lower values of both *RMSE* and *ME* compared to other heights. It is demonstrated that the WRF simulation

using Setup3 as a parameterization scheme is better for the study area, especially at an altitude of 50 m.

3.2. Results of LSTM Neural Network Wind Speed Prediction

This section focuses on the results of wind speed prediction at multiple heights by building LSTM neural networks with added attention mechanisms. Firstly, the output data of the innermost nested domain d04 in the WRF simulation are processed. The inputs are taken as the inputs of the simulated wind speed, wind directions, and temperatures of the WRF simulation from 1 December to 22 at six heights, namely 50 m, 75 m, 100 m, 120 m, 140 m, and 150 m. The LSTM neural network model is established. Next, the variation characteristics among the wind speed influencing factors at different heights are learned by machine learning to analyze the influence of different categories of data on wind speed prediction, and the attention mechanism further explores the correlation among the data. Finally, wind speed is predicted for 23 December at different heights. The comparison of LSTM predicted wind speed and measured wind speed at each height is shown in Figure 8. The comparison of LSTM predicted mean wind profile and measured mean wind profile on 23 December is shown in Figure 9, respectively.

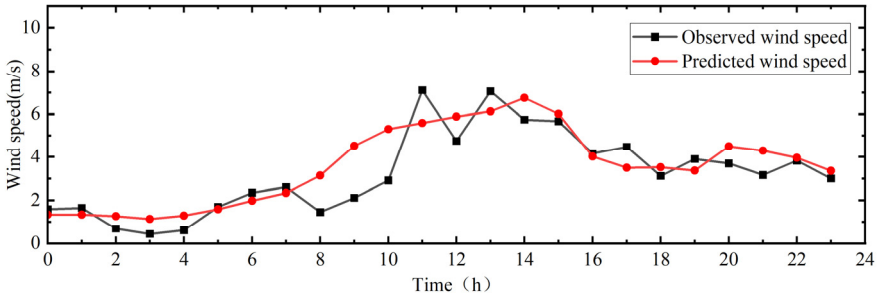

(**a**)

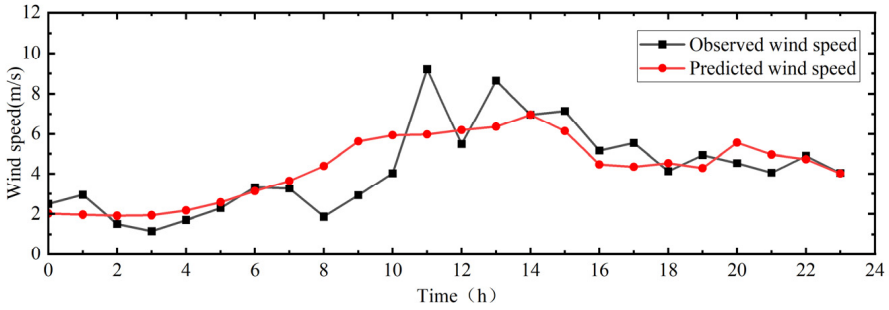

(**b**)

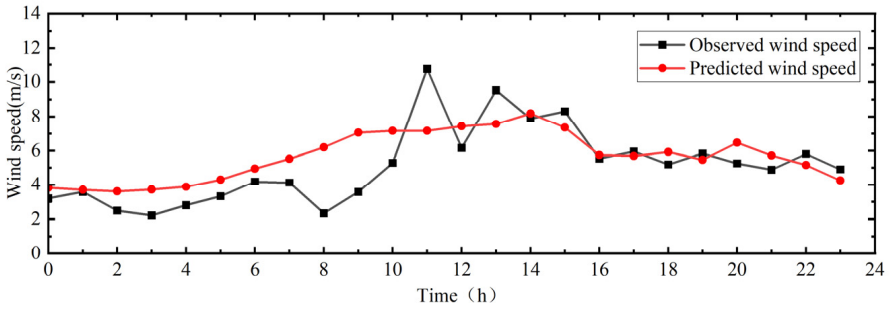

(**c**)

Figure 8. *Cont.*

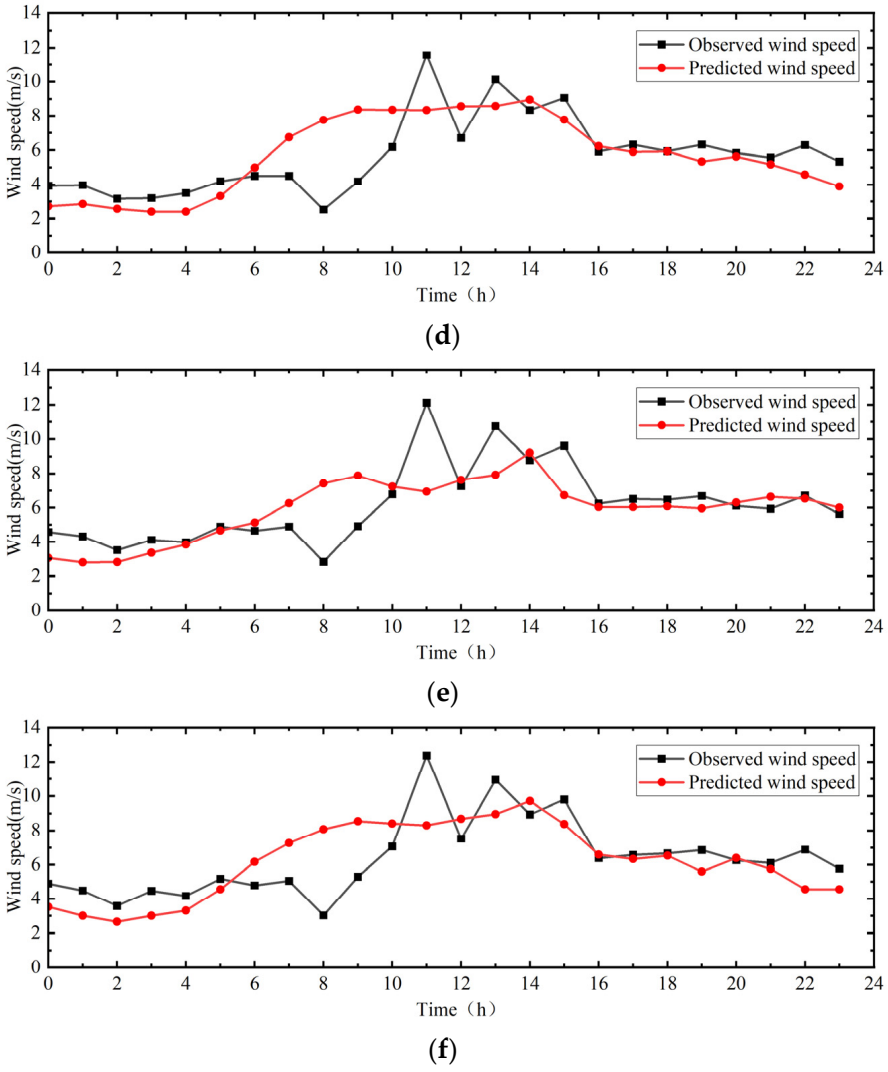

Figure 8. Comparison of LSTM predicted and observed wind speed at different heights (23 December): (**a**) 50 m, (**b**) 75 m, (**c**) 100 m, (**d**) 120 m, (**e**) 140 m, and (**f**) 150 m.

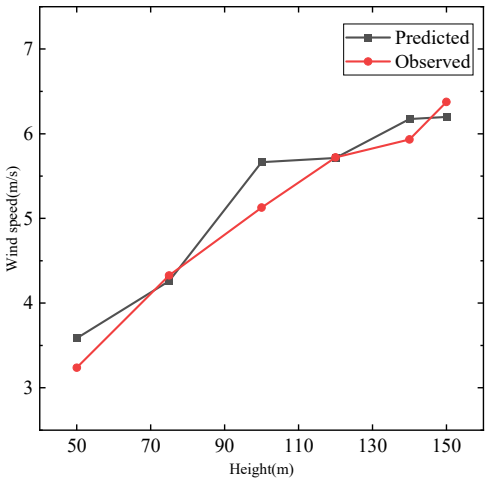

Figure 9. Comparison of LSTM predicted and observed wind profile.

From Figure 8a, it is evident that at a height of 50 m, the predicted wind speed shows minimal differences from the observed wind speed from 0:00 to 07:00 and from 15:00 to

23:00, with an error of less than 1 m/s. However, from 07:00 to 15:00, there is a slight discrepancy between the predicted and observed wind speeds, with an error of about 2 m/s. The peak value predicted by LSTM is 5.6 m/s, which is slightly lower than the peak value of the observed wind speed, but the trend of the wind speed curves is more consistent. From Figure 8b, it can be observed that at a height of 75 m, the observed wind speed curve reaches its daily peak at 11:00. However, the model fails to accurately predict the change of the wind speed at this moment, which leads to the maximum error between the predicted and observed wind speeds, which is about 3 m/s. From 0:00 to 7:00 and from 14:00 to 23:00, there are only minor differences between the predicted and observed wind speeds, with an error of less than 1 m/s. The forecast reached its maximum wind speed for the day at 14:00, which is slightly later than the actual situation. At a height of 100 m, the wind speed prediction is similar to that at 75 m. As can be seen in Figure 8d, at the height of 120 m, the predicted wind speed is lower than the observed wind speed from 0:00 to 6:00, and the trend and value of the predicted wind speed and the observed wind speed change from 15:00 to 21:00 are more in line with each other. However, from 6:00 to 8:00, the observed wind speed decreases slowly, but the model fails to predict this wind speed change and shows an increasing trend, resulting in the maximum error between the predicted and observed wind speeds, which is about 4 m/s. From Figure 8e,f, it can be seen that at the heights of 140 m and 150 m, the effect of wind speed prediction is similar to that at the height of 75 m. There is an error of about 1 m/s between the predicted and observed wind speeds from 0:00 to 7:00 and from 16:00 to 23:00, but the predicted wind speed curve is smoother compared to the measured one, and it fails to accurately predict the change of wind speeds that decreases first and then increases from 8:00 to 16:00.

Overall, the wind speed trends and values predicted by the LSTM at different heights are more in line with the actual measurements, and the best predictions are made at the heights of 50 and 75 m. However, the model predicted wind speed curves are smoother than those of the actual measurements, and the peak values are not obvious enough. This is because the model is more concerned with capturing the long-term dependence and the overall trend of the input data during the learning process, resulting in some short-term fluctuations not being emphasized. In addition, the attention mechanism introduced for weight allocation amplifies the important parts and ignores irrelevant disturbances, but this may also lead to the neglect of local peaks so that the predicted wind speed fails to reflect the changes of peaks with clarity.

As can be seen in Figure 9, the LSTM predicted average wind speeds at 50 m, 100 m, and 140 m heights on 23 December are slightly larger than the observed average wind speeds, the observed average wind speeds at a height of 150 m are slightly larger than the LSTM predicted average wind speeds, and the predicted average wind speeds at a height of 75 m are nearly the same as the observed average wind speeds. Overall, the predicted and observed mean wind speeds at each height coincide with each other in terms of trend, and there are slight differences in values, except that the error between the predicted and measured mean wind speeds at the height of 100 m is 0.54 m/s, while the errors of wind speeds at other heights are all within 0.3 m/s. It is shown that the established LSTM model has better wind speed prediction effects at heights from 50 to 150 m, and the accuracy of the prediction results is high, which can be used in combination with the WRF as a short-term wind speed prediction in forested regions with complex terrain.

3.3. Assessment of Wind Energy Resources

Affected by the height of trees in the forest area, there are certain limitations in the development and utilization of wind energy at near-ground levels, and the hub height of wind turbines in wind farms currently under construction has exceeded 100 m, so it is of practical significance to evaluate and develop the wind energy at the heights of 100 m and above. Based on the WRF simulation results, an assessment of the Weibull distribution parameters for wind speeds at heights of 100 m and 150 m is conducted. The Weibull distribution curves of the WRF simulation results and the observation results at each height

are shown in Figure 10. The results of the calculation of the Weibull distribution parameters of the WRF simulation values and the observation values at each height are shown in Table 2.

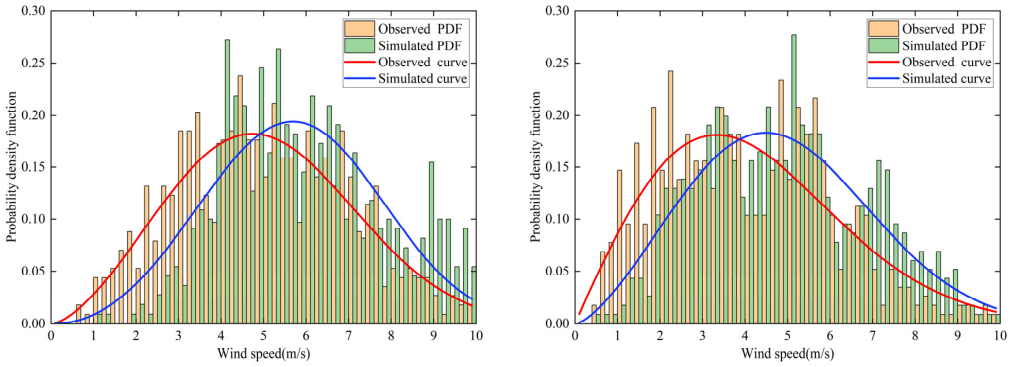

Figure 10. Weibull probability density distribution curves for different heights: (**a**) 100 m and (**b**) 150 m.

Table 2. Parameter and error of the Weibull distribution at different heights.

Height	**100 m**			**150 m**		
	Observation	Simulation	Error	Observation	Simulation	Error
k	2.00	2.50	0.50	2.60	3.19	0.59
c	4.73	5.51	16.5%	5.72	6.40	11.89%

As can be seen in Figure 10, the WRF simulated fitted curves are shifted to the right compared to the observed probability density fitted curves, which indicates that the model underestimates the frequency density of low wind speeds and overestimates that of high wind speeds, resulting in an overestimation of the WRF for the value of wind speeds in the study area. In addition, from the specific data analysis, as seen in Table 2, the error in the shape parameter k between the simulated and measured fitting curves for each height is around 0.5. The relative error of the scale parameter c is within a 20% error margin. Currently, there are no clearly defined error margins for specific parameters in the Weibull probability density distribution for wind energy assessment. Acceptable error levels vary depending on the specific application, complexity of the terrain, and the simulation method used. For complex terrain forest regions, our relative error values are within acceptable limits [42]. The relative error values are within the acceptable range, and both of the Weibull distribution parameters for 150 m have smaller relative errors compared with those for 100 m. The results show that it is feasible to carry out wind resource assessment in the study area based on the WRF simulation results, especially at a height of 150 m.

The distribution of monthly average wind power density levels for the innermost nested domain at 100 and 150 m heights for the December 2020 WRF simulation is shown in Figure 11.

As can be seen in Figure 11, the wind power density in the forested area of complex terrain and the surrounding area at the height of 100 m is mostly between 40 and 160 W/m^2, while the wind power density in the forested area of complex terrain and the surrounding area at the height of 150 m is mostly between 140 and 300 W/m^2, and there are also many areas with more than 300 W/m^2. This shows that the average wind power density increases with the increase in height; moreover, combined with the simulation results of Weibull distribution parameters, the wind energy resources at the height of 150 m in the study religion are better than those at a height of 100 m, and it is more suitable for the development and utilization of wind energy resources.

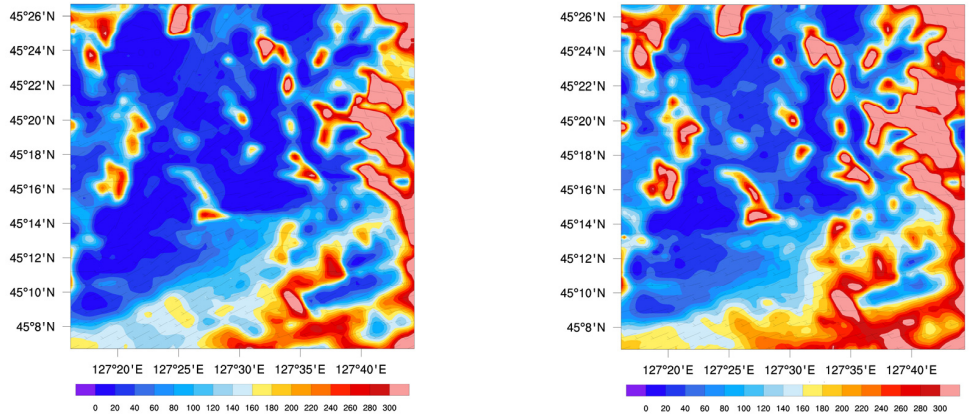

Figure 11. Mean wind power density maps for December from different heights: (**a**) 100 m and (**b**) 150 m.

4. Conclusions

This study aims to select the optimal combination of parameterization schemes for WRF to accurately assess the wind field characteristics of the forested area with complex terrain and to perform short-term wind speed prediction for each height wind speed simulation value with the LSTM-Attention neural network and, finally, to perform the wind energy resource assessment of the selected area. The results of this study are expected to provide methodological support for the development of wind energy resources and the siting of wind farms in forested regions. The main conclusions are as follows:

(1) In the WRF model, the combination and selection of parameterization schemes greatly impact the near-surface wind field, especially in the forested region. By selecting multiple schemes, the comparison reveals that the settings of the YSU planetary boundary layer scheme and MM5 surface layer scheme are selected to simulate the best effect. By setting it as the parameterized scheme for the selected study area, it is found that the WRF is more effective in simulating the wind field at heights of 50 m and above, with the wind speed values and trends matching, while those below 50 m corresponding to the measured data only in terms of the trend due to the influence of the trees on the ground surface.

(2) By inputting the simulation results of the innermost nested domain of the WRF into the LSTM neural network and introducing the attention mechanism, the established wind speed prediction models at six different heights from 50 m to 150 m were compared with the measured wind speeds, and the predicted values compared well with the measured values. Furthermore, the change trends and specific values did not differ much, except for the 100 m height, where the error between the predicted average wind speeds and measured average wind speeds was 0.54 m/s. However, the other heights were all within 0.3 m/s, which was lower than the current wind speed simulation error in the forest region. It is proved that the established LSTM-Attention model can be used for short-term wind speed prediction in complex forest areas, which can provide a preliminary technical guarantee for the site selection of wind farms in complex terrain.

(3) Based on the WRF simulation results, wind energy resources are evaluated for wind speeds at the heights of 100 m and 150 m. The Weibull distribution curves and parameters at 100 m and 150 m are compared with the measured values. The errors of the curves and parameters at the height of 150 m are relatively small compared with those of the measured values. Combined with the WRF simulation results and the calculation of the average wind power density in December in the study area, it is proved that the wind energy resources at a height of 150 m are relatively rich and suitable for developing and utilizing wind energy resources.

Author Contributions: Conceptualization, D.Z. and R.W.; methodology, G.C.; software, G.C.; validation, G.C. and L.Z.; formal analysis, G.C. and D.Z.; data curation, G.C. and R.W.; writing—original draft preparation, G.C. and H.Z.; writing—review and editing, G.C., L.Z. and H.Z.; visualization, G.C.; supervision, D.Z. and R.W.; project administration, D.Z., L.Z., H.Z. and S.Y.; funding acquisition, S.Y. All authors have read and agreed to the published version of the manuscript.

Funding: This research was supported by the China National Key R&D Program (2022YFB2602102) and the Heilongjiang Provincial Natural Science Foundation (Grant No. LH2020E067).

Institutional Review Board Statement: Not applicable.

Informed Consent Statement: Not applicable.

Data Availability Statement: Data can be obtained from the authors upon request.

Conflicts of Interest: The authors declare no conflicts of interest.

References

1. Wen, J.H.; Zhou, L.; Zhang, H.F. Mode interpretation of blade number effects on wake dynamics of small-scale horizontal axis wind turbine. *Energy* **2023**, *263*, 13. [CrossRef]
2. Sahin, A.D. Progress and recent trends in wind energy. *Prog. Energy Combust. Sci.* **2004**, *30*, 501–543. [CrossRef]
3. Roga, S.; Bardhan, S.; Kumar, Y.; Dubey, S.K. Recent technology and challenges of wind energy generation: A review. *Sustain. Energy Technol. Assess.* **2022**, *52*, 17. [CrossRef]
4. Hu, W.C.; Yang, Q.S.; Chen, H.P.; Yuan, Z.T.; Li, C.; Shao, S.; Zhang, J. Wind field characteristics over hilly and complex terrain in turbulent boundary layers. *Energy* **2021**, *224*, 14. [CrossRef]
5. Lu, H.Y.; Zhou, L.; Wen, J.H.; Tang, H.; Guo, P.; Tse, T.K.T.; Zhang, H.F. Aerodynamic performance improvements for a Savonius turbine above a forward-facing step via inclined solar panel: A computational study. *J. Clean. Prod.* **2023**, *413*, 12. [CrossRef]
6. Liu, X.G.; Cao, J.L.; Xin, D.B. Wind field numerical simulation in forested regions of complex terrain: A mesoscale study using WRF. *J. Wind Eng. Ind. Aerodyn.* **2022**, *222*, 11. [CrossRef]
7. Wilson, J.D. Measured and modelled wind variation over irregularly undulating terrain. *Agric. For. Meteorol.* **2018**, *249*, 187–197. [CrossRef]
8. Zhang, J.A.; Liu, D.; Li, Z.J.; Han, X.; Liu, H.; Dong, C.; Wang, J.Y.; Liu, C.Y.; Xia, Y.P. Power prediction of a wind farm cluster based on spatiotemporal correlations. *Appl. Energy* **2021**, *302*, 10. [CrossRef]
9. Cepeda, A.C.; Rios, M.A. Bulk power system availability assessment with multiple wind power plants. *Int. J. Electr. Comput. Eng.* **2021**, *11*, 27–36. [CrossRef]
10. Kosar, O.; Özgür, M.A. Wind energy resource assessment of Kutahya, Turkey using WAsP and layout optimization. *Proc. Inst. Mech. Eng. Part A J. Power Energy* **2021**, *235*, 629–640. [CrossRef]
11. Zhou, L.; Wen, J.H.; Wang, Z.K.; Deng, P.R.; Zhang, H.F. High-fidelity wind turbine wake velocity prediction by surrogate model based on d-POD and LSTM. *Energy* **2023**, *275*, 14. [CrossRef]
12. Zhang, H.F.; Wen, J.H.; Zhan, J.; Xin, D.B. Effects of blade number on the aerodynamic performance and wake characteristics of a small horizontal-axis wind turbine. *Energy Conv. Manag.* **2022**, *273*, 16. [CrossRef]
13. Gharaati, M.; Xiao, S.L.; Wei, N.J.; Martínez-Tossas, L.A.; Dabiri, J.O.; Yang, D. Large-eddy simulation of helical- and straight-bladed vertical-axis wind turbines in boundary layer turbulence. *J. Renew. Sustain. Energy* **2022**, *14*, 24. [CrossRef]
14. Yang, X.L.; Pakula, M.; Sotiropoulos, F. Large-eddy simulation of a utility-scale wind farm in complex terrain. *Appl. Energy* **2018**, *229*, 767–777. [CrossRef]
15. Prósper, M.A.; Otero-Casal, C.; Fernández, F.C.; Miguez-Macho, G. Wind power forecasting for a real onshore wind farm on complex terrain using WRF high resolution simulations. *Renew. Energy* **2019**, *135*, 674–686. [CrossRef]
16. Tuy, S.; Lee, H.S.; Chreng, K. Integrated assessment of offshore wind power potential using Weather Research and Forecast (WRF) downscaling with Sentinel-1 satellite imagery, optimal sites, annual energy production and equivalent CO_2 reduction. *Renew. Sust. Energ. Rev.* **2022**, *163*, 19. [CrossRef]
17. Xu, W.F.; Liu, P.; Cheng, L.; Zhou, Y.; Xia, Q.; Gong, Y.; Liu, Y.N. Multi-step wind speed prediction by combining a WRF simulation and an error correction strategy. *Renew. Energy* **2021**, *163*, 772–782. [CrossRef]
18. Quimbayo-Duarte, J.; Wagner, J.; Wildmann, N.; Gerz, T.; Schmidli, J. Evaluation of a forest parameterization to improve boundary layer flow simulations over complex terrain. A case study using WRF-LES V4.0.1. *Geosci. Model Dev.* **2022**, *15*, 5195–5209. [CrossRef]
19. Sun, W.J.; Zhou, S.Y.; Yang, J.S.; Gao, X.Q.; Ji, J.L.; Dong, C.M. Artificial Intelligence Forecasting of Marine Heatwaves in the South China Sea Using a Combined U-Net and ConvLSTM System. *Remote Sens.* **2023**, *15*, 21. [CrossRef]
20. Jörges, C.; Berkenbrink, C.; Stumpe, B. Prediction and reconstruction of ocean wave heights based on bathymetric data using LSTM neural networks. *Ocean Eng.* **2021**, *232*, 18. [CrossRef]
21. Yu, R.G.; Gao, J.; Yu, M.; Lu, W.H.; Xu, T.Y.; Zhao, M.K.; Zhang, J.; Zhang, R.X.; Zhang, Z. LSTM-EFG for wind power forecasting based on sequential correlation features. *Futur. Gener. Comp. Syst.* **2019**, *93*, 33–42. [CrossRef]

22. Skamarock, W.; Klemp, J.; Dudhia, J.; Gill, D.; Liu, Z.; Berner, J.; Huang, X. *A Description of the Advanced Research WRF Model Version 4.3*; NCAR Tech Note, NCAR/TN–556+ STR; National Center for Atmospheric Research: Boulder, CO, USA, 2021. [CrossRef]
23. Giannakopoulou, E.M.; Nhili, R. WRF Model Methodology for Offshore Wind Energy Applications. *Adv. Meteorol.* **2014**, *2014*, 14. [CrossRef]
24. National Centers for Environmental Prediction; National Weather Service; NOAA; U.S. Department of Commerce. *NCEP FNL Operational Model Global Tropospheric Analyses, Continuing from July 1999*; Research Data Archive at the National Center for Atmospheric Research, Computational and Information Systems Laboratory: Boulder, CO, USA, 2000. [CrossRef]
25. Zängl, G.; Gohm, A.; Obleitner, F. The impact of the PBL scheme and the vertical distribution of model layers on simulations of Alpine foehn. *Meteorol. Atmos. Phys.* **2008**, *99*, 105–128. [CrossRef]
26. Kain, J.S. The Kain–Fritsch convective parameterization: An update. *J. Appl. Meteorol. Climatol.* **2004**, *43*, 170–181. [CrossRef]
27. Iacono, M.J.; Delamere, J.S.; Mlawer, E.J.; Shephard, M.W.; Clough, S.A.; Collins, W.D. Radiative forcing by long-lived greenhouse gases: Calculations with the AER radiative transfer models. *J. Geophys. Res. Atmos.* **2008**, *113*, 8. [CrossRef]
28. Kain, J.S.; Fritsch, J.M. A one-dimensional entraining/detraining plume model and its application in convective parameterization. *J. Atmos. Sci.* **1990**, *47*, 2784–2802. [CrossRef]
29. Mlawer, E.J.; Taubman, S.J.; Brown, P.D.; Iacono, M.J.; Clough, S.A. Radiative transfer for inhomogeneous atmospheres: RRTM, a validated correlated-k model for the longwave. *J. Geophys. Res. Atmos.* **1997**, *102*, 16663–16682. [CrossRef]
30. Hong, S.Y.; Noh, Y.; Dudhia, J. A new vertical diffusion package with an explicit treatment of entrainment processes. *Mon. Weather Rev.* **2006**, *134*, 2318–2341. [CrossRef]
31. Jiménez, P.A.; Dudhia, J.; González-Rouco, J.F.; Navarro, J.; Montávez, J.P.; García-Bustamante, E. A Revised Scheme for the WRF Surface Layer Formulation. *Mon. Weather Rev.* **2012**, *140*, 898–918. [CrossRef]
32. Janjić, Z.I. The step-mountain eta coordinate model: Further developments of the convection, viscous sublayer, and turbulence closure schemes. *Mon. Weather. Rev.* **1994**, *122*, 927–945. [CrossRef]
33. Janić, Z.I. *Nonsingular Implementation of the Mellor-Yamada Level 2.5 Scheme in the NCEP Meso Model*; National Centers for Environmental Prediction: College Park, GA, USA, 2001.
34. Mukul Tewari, N.; Tewari, M.; Chen, F.; Wang, W.; Dudhia, J.; LeMone, M.; Mitchell, K.; Ek, M.; Gayno, G.; Wegiel, J. Implementation and verification of the unified NOAH land surface model in the WRF model (Formerly Paper Number 17.5). In Proceedings of the 20th Conference on Weather Analysis and Forecasting/16th Conference on Numerical Weather Prediction, Seattle, WA, USA, 10–15 January 2004.
35. Niu, G.Y.; Yang, Z.L.; Mitchell, K.E.; Chen, F.; Ek, M.B.; Barlage, M.; Kumar, A.; Manning, K.; Niyogi, D.; Rosero, E.; et al. The community Noah land surface model with multiparameterization options (Noah-MP): 1. Model description and evaluation with local-scale measurements. *J. Geophys. Res. Atmos.* **2011**, *116*, D12109. [CrossRef]
36. Hong, S.-Y.; Lim, J.-O.J. The WRF Single-Moment 6-Class Microphysics Scheme (WSM6). *Asia-Pac. J. Atmos. Sci.* **2006**, *42*, 129–151.
37. Hochreiter, S.; Schmidhuber, J. *LSTM Can Solve Hard Long Time Lag Problems*; MIT Press: Cambridge, MA, USA, 1996; Volume 9.
38. Gers, F.A.; Schmidhuber, J.; Cummins, F. Learning to forget: Continual prediction with LSTM. *Neural Comput.* **2000**, *12*, 2451–2471. [CrossRef] [PubMed]
39. Serban, A.; Paraschiv, L.S.; Paraschiv, S. Assessment of wind energy potential based on Weibull and Rayleigh distribution models. *Energy Rep.* **2020**, *6*, 250–267. [CrossRef]
40. Zheng, H.B.; Huang, W.F.; Zhao, J.H.; Liu, J.F.; Zhang, Y.Y.; Shi, Z.; Zhang, C.H. A novel falling model for wind speed probability distribution of wind farms. *Renew. Energy* **2022**, *184*, 91–99. [CrossRef]
41. Maatallah, T.; El Alimi, S.; Dahmouni, A.W.; Ben Nasrallah, S. Wind power assessment and evaluation of electricity generation in the Gulf of Tunis, Tunisia. *Sust. Cities Soc.* **2013**, *6*, 1–10. [CrossRef]
42. Fernández-González, S.; Martín, M.L.; García-Ortega, E.; Merino, A.; Lorenzana, J.; Sánchez, J.L.; Valero, F.; Rodrigo, J.S. Sensitivity Analysis of the WRF Model: Wind-Resource Assessment for Complex Terrain. *J. Appl. Meteorol. Climatol.* **2018**, *57*, 733–753. [CrossRef]